Paper ID: ETC2023-303 Proceedings of 15th European Conference on Turbomachinery Fluid dynamics & Thermodynamics
ETC15, April 24-28, 2023; Budapest, Hungary
DOI: 10.2514/1.I011171.

FAN-INTAKE AERODYNAMIC INTERACTIONS UNDER CROSSWIND CONDITIONS

L. Boscagli - D. MacManus - R. Christie

Cranfield University, MK43 0AL, Cranfield, UK
luca.boscagli@cranfield.ac.uk

ABSTRACT

The aerodynamics of an aero-engine intake under off-design conditions is characterized by a range of steady and unsteady mechanisms that can adversely affect the fan operability. A hierarchical computational fluid dynamics approach was used for an initial assessment of the primary aerodynamic interactions between the fan and the intake design. These approaches included steady computations with a lower order fan model as well as full unsteady computations. For a powered intake in crosswind, the direction of the wind determines the direction of rotation of the ground vortex relative to the fan. For the full unsteady analyses, the threshold crosswind speed reduced by 12kts and 22kts relative to the steady analysis for the counter-rotating and co-rotating configuration respectively. Overall, this work identified and assessed for the first time a fan-intake unsteady aerodynamic interactions that may affect the design of short intakes in association with fan systems.

KEYWORDS

Turbofan, CFD, Unsteady, Ground-vortex, SBLI

INTRODUCTION

An aero-engine which operates at maximum power near the ground may be subject to a complex three dimensional flow field within the intake due to shock-wave boundary layer interactions (SBLI) on the intake lip as well as the development of a ground vortex due to the proximity of the engine to the ground (Fig. 1). Under crosswind conditions, the stagnation line of the engine captured streamtube is located on the external cowl of the nacelle. On the windward side, the flow undergoes a significant acceleration around the nacelle leading edge, which can lead to a supersonic region on the intake lip which terminates with a near-normal shock wave. The notable adverse pressure gradient ($dp/dx > 0$) through the shock can separate the intake boundary layer and lead to a significant separation and total pressure distortions that can limit the fan operability. For ultra-high bypass ratio aero-engines, the compactness of the nacelle is likely to increase and lead to a more close-coupled interaction between the fan and the intake flow field. Thus, the unsteady aerodynamic mechanisms that limits the design of short aero-engine intakes need to be understood.

Previous experimental and computational investigations (Trapp and Da Motta Girardi [2010], Murphy and MacManus [2011]) of a cylindrical intake in near ground operations revealed the influence of crosswind velocity, ground clearance and approaching boundary layer profile on the characteristics of the ground vortex. Relative to crosswind conditions the strength of the ground vortex is mainly a function of the non-dimensional ground clearance (H/D_{hi}) and the ratio between the velocity at the intake highlight plane and the crosswind velocity ($U^* = U_{hi}/V_{wind}$).

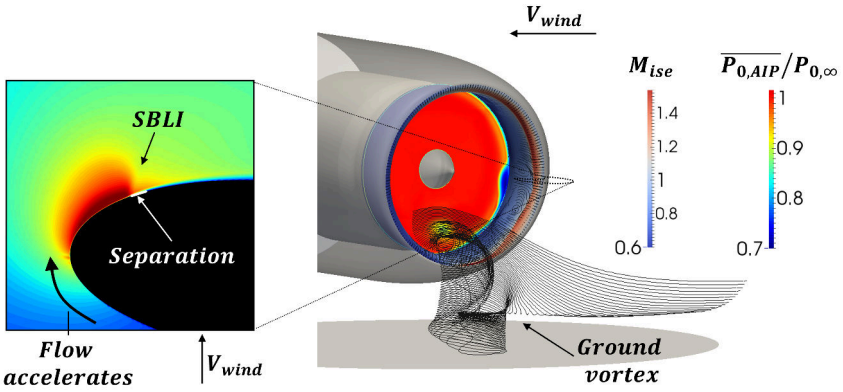

Figure 1: **Schematic of the aerodynamics of an aero-engine intake under crosswind conditions**

Thus, when either the ground clearance or U^* are sufficiently great (Murphy and MacManus [2011]), there is no interaction of the ingested engine streamtube with the ground and therefore the ground vortex does not arise. Recent computational analysis (Awes et al. [2020]) of an isolated modern turbofan demonstrator revealed a reduction of up to 8% in fan stall margin due to ground vortex like distortions. Lee et al. [2019] showed for a fan-intake coupled configuration under crosswind conditions, that when the ground vortex is not taken into account the fan is more tolerant to intake total pressure distortions when the fan rotational speed is increased. Recent investigations (Boscagli et al. [2022]) identified a strong coupled interaction between the fan and a short intake for an aero-engine under crosswind conditions. The impact of fan unsteadiness can augment the amplitude of the axial pulsations for a transonic SBLI which adversely affects the separation onset of the intake boundary layer. Hodder [1976] assessed the effect of the ground vortex on fan tonal noise within an aero-engine intake operating at maximum take-off power. The ground vortex augmented the amplitude of blade passing frequency content by 4-6db. However, there were no shock-waves within the intake and the effect of the increased fan tonal noise on the separation onset of the intake boundary layer was not determined. Page et al. [2018] assessed the effect of co- and contra-rotating vortices (Fig. 2) on the stall margin of a transonic fan for S-duct applications. Both vortex patterns did not produce any destabilizing effect on the rotor. For a short podded intake there is currently no evidence in the literature on how a change in crosswind direction or fan rotational speed affects the intake flow separation mechanisms and the interaction with the fan. Within this context, the aim of this work is to provide an initial assessment of the aerodynamic interactions between the fan and the intake which limit the design of short aero-engine intakes.

METHODOLOGY

HYDRA (Moinier [1999], Lapworth [2004]) was used as a CFD solver. Steady RANS analysis with a lower order fan model (IBMSG, Cao et al. [2017a]) and full-unsteady computations (URANS-TRF) with a sliding-plane boundary conditions (Fig. 3) were used to determine and quantify the primary aerodynamic interactions between the fan and the intake. The IBMSG model uses an infinite number of smeared fan blades to replicate the parallel and normal forces exchanged between the blade and the flow. The approach considerably reduces the computational size and cost of the computations. However, the azimuthal variation of the static pres-

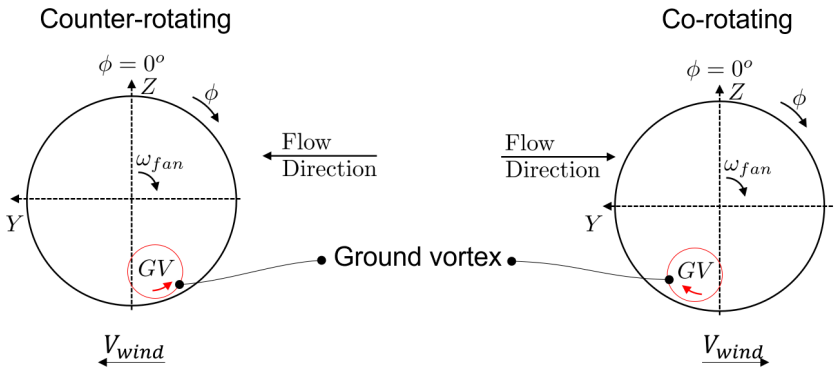

Figure 2: **Schematic of co-rotating and counter-rotating crosswind configurations**

sure field upstream of the fan due to the rotating fan blades is not taken into account in the IBMSG model. Validation with experimental data and steady and unsteady CFD verification with mixing-plane and sliding-plane approaches were previously done for the IBMSG model (Cao et al. [2017b], Cui et al. [2019], Ma et al. [2019]). The test cases included a transonic rotor with and without inlet distortions and fan-intake coupled analyses at maximum take-off (high engine incidence angle) conditions. Overall, the IBMSG model was able to capture the radial mass flow redistribution upstream of the fan, although the wake downstream of the fan was significantly thicker due to stronger shock losses within the blade passage relative to the fully-resolved fan computations. For consistency with previous work on IBMSG, the turbulence model was Spalart-Allmaras (Spalart and Allmaras [1994]), with a turbulent kinetic energy production term based on both strain and vorticity. Previous work (Bron [2002]) showed that, relative to experiments, RANS methods with linear eddy viscosity turbulence models are able to predict the unsteady interaction between SBLI and upstream travelling acoustic perturbations. All the walls of the computational domain (Fig. 3) were treated as viscous walls and farfield boundary conditions were used to control the crosswind speed. The edges of the computational domain were positioned at about $35D_{fan}$ upstream of the intake, which is sufficiently far based on previous work (Zantopp et al. [2010], Lee et al. [2019]). The computational domain included a viscous ground wall below the intake to capture the interaction of the fan with the ground vortex. In agreement with previous work (Zantopp et al. [2010]), the ground boundary layer freely developed from the computational domain boundaries. A typical (Hall and Hynes [2006]) non dimensional ground clearance ($H/D_{hi} \approx 0.95$, Fig. 3) for large bypass ratio turbofan engines was used. The mass flow through the intake was prescribed at the engine outlet boundaries through mass-flow outlet boundary conditions to achieve a nominal fan capacity ($Q_{fan,ref}$). The CFD methodology used in this paper was previously validated (Boscagli et al. [2022]) for an unpowered intake in crosswind and for a single stage fan. The grids for the analyses with the lower order fan model and with the sliding-plane approach were fully structured and had about 14×10^6 and 42×10^6 nodes respectively. The analyses were sufficiently grid and domain independent. The threshold crosswind speed ($V_{wind,c}$) of the intake was determined as the highest V_{wind} with no reverse mass flow at the Aerodynamic Interface Plane (AIP) which was positioned $0.05r_{fan}$ upstream of the blade tip leading edge. For the unsteady computations 60 timesteps per blade-passing were used (Carnevale et al. [2017]) and the simulations were initialised with steady RANS at the corresponding operating conditions. The computations were

advanced in time for a minimum of 6 fan revolutions after the initial numerical transient.

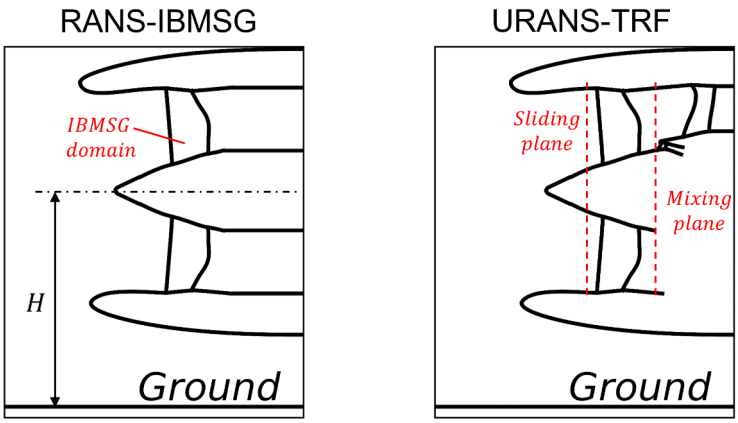

Figure 3: **Schematic of the CFD domains and definition of ground clearance**

Data analysis

The total pressure distortions at the AIP were quantified based on $DC60$ (Eq. 1). $DC60$ indicates the maximum loss in area-averaged total pressure within a $60°$ sector ($\overline{P_{0,60}} - \overline{P_{0,AIP}}$) as a fraction of the local dynamic head ($\overline{q_{AIP}}$) that the fan may be able to tolerate. The metric is a typical industrial criterion to determine the operating limits of the fan on the basis of the assumptions of parallel compressor theory (Reid [1969]). However, for vortical flows is not useful to establish the design limits of the aero-engine intake due to the highly non-monotonic behaviour (Murphy and MacManus [2011]). Furthermore, DC60 is a total pressure distortion metric and, in the presence of a ground vortex, it is not fully indicative of flow separation. In this work the focus is on the separation onset of the boundary layer within the intake and therefore this was evaluated based on the percentage of reverse mass flow relative to the overall mass flow through the AIP ($\dot{m}^{-}[\%]$) and a threshold crosswind velocity ($V_{wind,c}$) was established based on $\dot{m}^{-} < 0.001\%$. Relative to RANS-IBMSG, URANS-TRF computations provide an indication of the impact of intake flow unsteadiness and fan upstream perturbations on the separation onset and characteristics of the intake boundary layer. The combination of the two effects (intake flow and fan unsteadiness) defines the reduction on the threshold crosswind velocity ($V_{wind,c}$) relative to the design method (RANS-IBMSG). Nevertheless, it is a hierarchical set of assessment and it is not intended as a flow decomposition. For each computational model, the intake design is evaluated relative to the requirements of a threshold reference crosswind speed ($V_{wind,ref}$, Eq. 2).

$$DC60 = \frac{\overline{P_{0,60}} - \overline{P_{0,AIP}}}{\overline{q_{AIP}}} \tag{1}$$

$$\Delta V_{wind} = V_{wind,c} - V_{wind,ref} \tag{2}$$

The non-dimensional circulation of the core of the ground vortex at the AIP ($\Gamma^* = \Gamma / U_{hi} D_{hi}$) was computed using the vorticity disk method approach (Van Der Wall and Richard [2005])

where the centre of the core of the ground vortex was selected based on the maximum value of signed axial vorticity. Although at the AIP the flow field is resolved within the absolute reference of frame, relative quantities were computed a posteriori based on a velocity triangle decomposition (Migliorini et al. [2021]). The unsteady characteristics of the intake flow field were quantified through a discrete Fourier decomposition and banded Fourier spectra were used to identify the spatial distribution of the unsteady fluctuations. For the coupled intake-fan configurations (URANS-TRF) the flow field is characterised by both high frequency and low frequency content associated with the blade-passing (f_{bp}) and the unsteadiness of the shock (Vadlamani et al. [2019]) and the ground vortex ($f < 0.1 f_{bp}$), respectively. To identify the spectral gap between the low and high frequencies, the frequency resolution of each band was $f_{bp}/10$. Within each band, the maximum amplitude of the fluctuations was used to quantify the unsteady content and enable a comparison between different operating conditions.

RESULTS AND DISCUSSION

A non-axisymmetric short intake ($L_{in}/D_{fan} = 0.35$) with a fixed ground clearance ($H/D_{hi} \approx 0.95$) was used. The case study investigated the impact of fan rotational speed and crosswind direction on the modulation of amplitude and space-time characteristics of the fan upstream pulsations. Relative to other intake designs, this particular design had a significantly greater pre-shock Mach number. Consequently, within the design intent this is expected to emphasize the unsteady adverse effect of fan-intake interaction (Boscagli et al. [2022]) on the threshold crosswind speed of the intake.

Effect of fan rotational speed

Previous work (Boscagli et al. [2022]) showed a notable unsteady adverse interaction between the upstream perturbations from the fan and the shock on the intake lip. Under undistorted inlet conditions, the amplitude of the fan perturbations tends to increase with an increase in loading at the tip of the fan blade. For the coupled fan-intake configuration, the effect of fan rotational speed ($N/\sqrt{T_{0,in}}$) was assessed for the counter-rotating configuration (Fig. 2) through a variation of the tip relative Mach number ($M_{tip,rel}$) with the engine mass flow held constant. Relative to the nominal intake design conditions ($Q_{fan,ref}$, $M^{ref}_{tip,rel}$) $M_{tip,rel}$ was increased and decreased by -0.02 and $+0.03$ respectively. The crosswind speed was progressively increased and the threshold crosswind speed ($V_{wind,c}$) for the intake was determined. Steady (RANS-IBMSG) and unsteady (URANS-TRF) computations were used to evaluate the combined effect of intake and fan unsteadiness on the intake threshold conditions. For the RANS-IBMSG, the threshold crosswind speed relative to the nominal design requirement ($V_{wind,ref}$) was $V_{wind,c} = V_{wind,ref} + 8kts$ and it was not affected by the change in fan rotational speed (Fig. 4). The approximate -0.02, $+0.03$ change in tip relative Mach number did not notably affect the upstream radial distribution of mass flux (Fig. 5) which is associated with the main beneficial steady effect of the fan on the intake threshold conditions (Boscagli et al. [2022]).

The combined effect of intake and fan unsteadiness on the intake threshold conditions was determined and quantified through the URANS-TRF model. Under the nominal intake design conditions ($Q_{fan,ref}$, $M^{ref}_{tip,rel}$) and based on the URANS-TRF model, the threshold crosswind velocity was $V_{wind,c} = V_{wind,ref} - 4kts$. Thus, the adverse effect of the unsteady fan-intake interaction reduced the $V_{wind,c}$ by $12kts$ relative to the RANS-IBMSG model. $N/\sqrt{T_{0,in}}$ was varied by about $\pm 3\%$ relative to the nominal design conditions and the tip relative Mach number

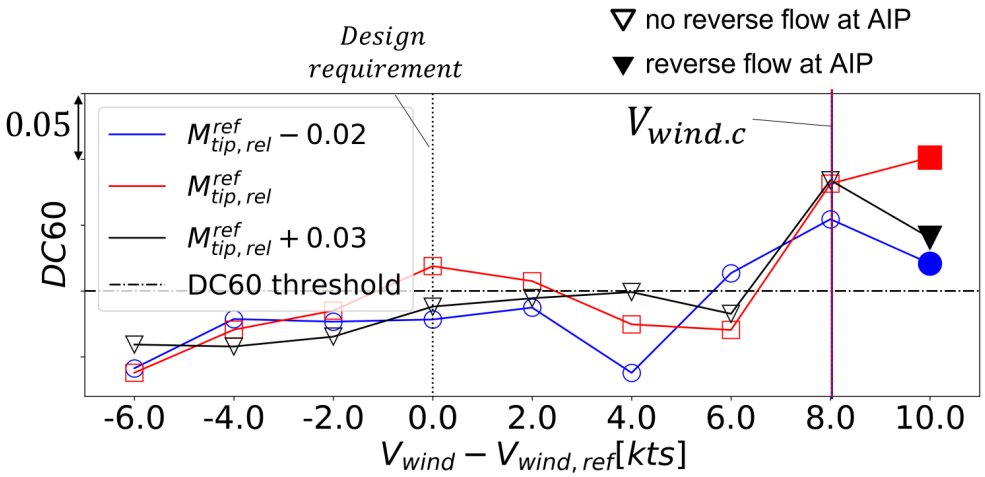

Figure 4: **Effect of fan rotational speed on DC60 at the AIP. The intake threshold crosswind velocity ($V_{wind,c}$) was determined based on no separation at the AIP. Steady RANS-IBMSG analyses, counter-rotating configuration**

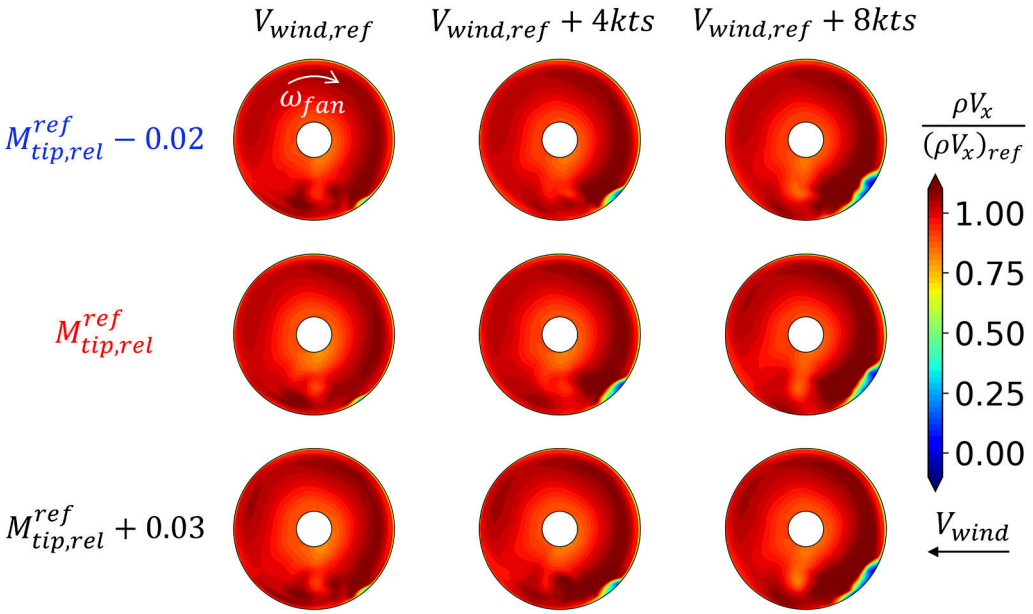

Figure 5: **Effect of fan rotational speed on non-dimensional mass flux at the AIP. Steady RANS computations with IBMSG (RANS-IBMSG), counter-rotating configuration**

varied by -0.02 and $+0.03$, respectively. Based on single stage isolated fan computations with mixing-plane boundary conditions, the estimated change in the amplitude of the azimuthal variation of the static pressure field (Δp) at the notional intake throat due to the change in fan rotational speed was about $\frac{\Delta p}{P_{0,\infty}} \approx \pm 0.1\%$ under clean conditions. However, the threshold crosswind velocity for the intake was not affected by the change in fan rotational speed. The non-uniformity of the intake flow field is also of interest. Thus, the azimuthal variation of

absolute Mach number further upstream of the fan and associated with the fan unsteadiness needs investigation (Boscagli et al. [2022]) and it is examined in the next paragraphs.

At the intake throat and at a radial position of $r/r_{fan} = 95\%$ (Fig. 6), the amplitude of the absolute Mach number azimuthal variation (ΔM) at blade-passing Engine-Order (EO) was different on the windward ($0° < \phi < 180°$) and on the leeward ($180° < \phi < 360°$) side of the intake. The blade-passing ΔM on the windward side increased from approximately 0.01 to 0.02 as the fan speed ($M_{tip,rel}$) increased from $M^{ref}_{tip,rel} - 0.02$ to $M^{ref}_{tip,rel} + 0.03$ as it was expected from the isolated fan computations. Conversely, on the leeward side ($180° < \phi < 360°$) ΔM was only slightly affected by a change in fan rotational speed and the amplitude was notably higher compared to the value estimated with the isolated fan stage computations which was approximately $\Delta M \approx 0.005$. The amplitude of the fan upstream pulsations is dominated by the strength of the ground vortex (approximately at $\phi = 180°$) as it notably increases the loading of the fan blade at the tip. Although at $M_{tip,rel} = M^{ref}_{tip,rel} - 0.02$ the amplitude of fan upstream pulsations slightly reduced relative to the datum ($M_{tip,rel} = M^{ref}_{tip,rel}$, Fig. 6b), the modulation of the unsteady static pressure field due to the fan was still sufficient to force the SBLI and cause an earlier onset of intake boundary layer separation relative to the RANS-IBMSG. Thus, the analysis did not identify the minimum threshold of blade-passing ΔM modulation that would reduce the adverse effect of fan unsteadiness on the threshold crosswind speed. The analysis further supported the evidence of an unsteady interaction mechanism between the ground vortex, the fan and the shock on the intake. The amplitude of the fan upstream pulsation is dominated by the interaction of the fan with the ground vortex. This is further explored in the next section where the effect of the crosswind direction on $V_{wind,c}$ is determined.

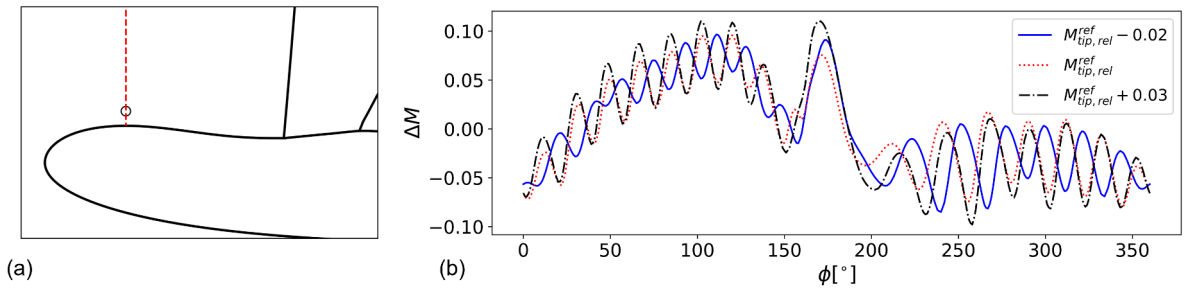

Figure 6: **(a) Schematic of the axial and radial position of the plot showed in (b); (b) time snapshot of azimuthal variation of absolute Mach number (ΔM) at $r/r_{fan} = 95\%$ and about $0.4r_{fan}$ upstream of the AIP. URANS-TRF at $V_{wind} = V_{wind,c}$**

Effect of crosswind direction

For a powered intake in crosswind, the direction of the wind determines the direction of rotation of the ground vortex relative to the fan. Thus, two different configurations can be distinguished (Fig. 2) which are referred to as co-rotating and counter-rotating. The impact of co-rotating and counter-rotating configurations on the threshold crosswind velocity of the intake was determined through both steady RANS-IBMSG and unsteady URANS-TRF computations. Thus, the combined effect of intake and fan unsteadiness on the threshold crosswind speed of the intake was assessed . The fan operated at the nominal design conditions, $M^{ref}_{tip,rel}$

and $Q_{fan,ref}$. Based on steady RANS-IBMSG model, the counter-rotating configuration had a threshold crosswind velocity that was $4kts$ lower than the co-rotating configuration based on a restrictive criterion of no reverse mass flow at the AIP (Fig. 7).

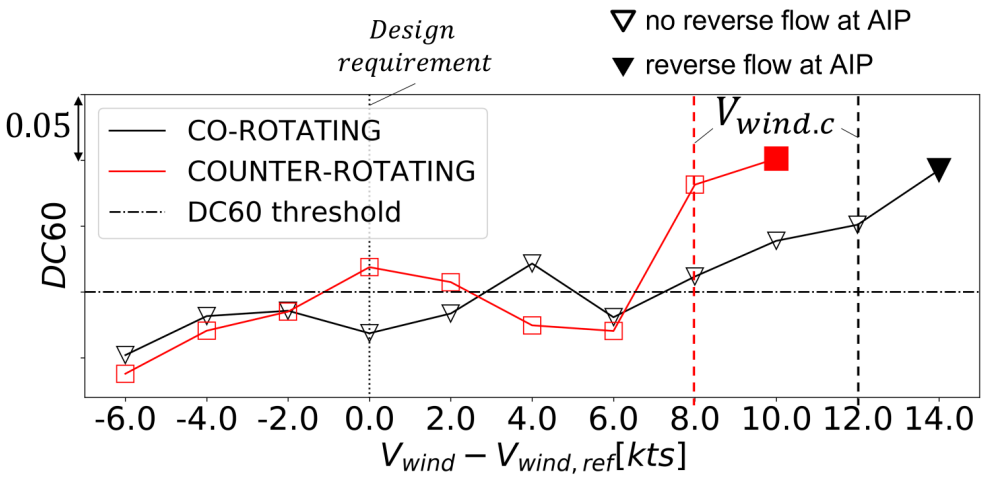

Figure 7: **Effect of crosswind velocity direction on DC60 at the AIP. The intake threshold crosswind velocity ($V_{wind,c}$) was determined based on no separation at the AIP. Steady RANS-IBMSG analyses**

The effect of the coupled intake and fan unsteadiness on the threshold crosswind velocity was further assessed. Under both configurations, the intake no longer met the nominal crosswind velocity requirement ($V_{wind,ref}$) when the unsteady fan-intake interaction was taken into account (Fig. 8). For the counter-rotating configuration the threshold crosswind velocity predicted by the URANS-TRF was $V_{wind,c} = V_{wind,ref} - 4kts$, whereas it was $V_{wind,c} = V_{wind,ref} - 10kts$ for the co-rotating configuration (Fig. 8). Thus, for the counter-rotating configuration the combined effect of intake and fan unsteadiness reduced $V_{wind,c}$ from $V_{wind,ref} + 8kts$ (RANS IBMSG) to $V_{wind,ref} - 4kts$ (URANS-TRF) with an overall $12kts$ penalty. For the co-rotating configuration $V_{wind,c}$ was reduced from $V_{wind,ref} + 12kts$ (RANS-IBMSG) to $V_{wind,ref} - 10kts$ (URANS-TRF) with an overall $22kts$ penalty. Based on the URANS-TRF model, the co-rotating configuration had a $V_{wind,c}$ which was $6kts$ lower relative to the co-rotating one. Thus, from an intake aerodynamic point of view the co-rotating configuration is more challenging based on the full-unsteady (URANS-TRF) computations. This is in disagreement with the steady RANS-IBMSG computations that had the opposite polarity (Fig. 7). Thus, this is of importance for an intake design process with steady RANS and with a threshold crosswind velocity condition which is based on the criteria for no reverse flow at the AIP.

The reason for the difference between steady RANS-IBMSG and URANS-TRF can be explained by the unsteady interaction between the fan pulsations and the shock on the intake lip. As showed in the previous section, the amplitude of the upstream pulsation of the fan is dominated by the ground vortex strength, position and relative orientation of the swirl flow onto the rotor. Based on the URANS-TRF computations, the counter-rotating configuration had a $V_{wind,c}$ that was $6kts$ greater than the co-rotating one (Fig. 8). Thus, the non-dimensional circulation of the ground vortex (Γ^*) was slightly greater for the counter-rotating case compared to the co-rotating one (Fig. 9). Nevertheless, the influence of the interaction between the ground vortex

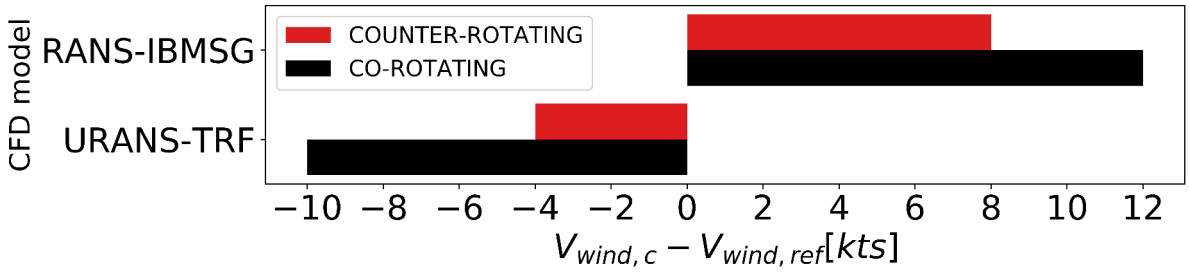

Figure 8: **Effect of crosswind direction on the threshold crosswind velocity ($V_{wind,c}$) for the steady RANS-IBMSG and the URANS-TRF models**

and the fan on the intake $V_{wind,c}$ was still greater for the co-rotating case.

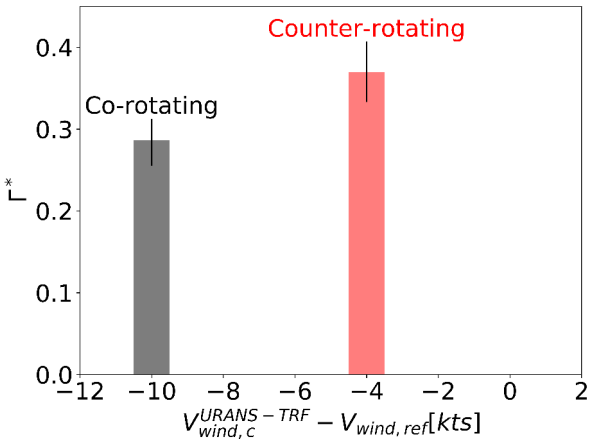

Figure 9: **Non-dimensional ground vortex circulation (Γ^*) for the co and counter-rotating configurations at their respective $V_{wind,c}$. URANS-TRF simulations**

The upstream propagation of the fan perturbations after the ground-vortex distortions (Fig. 10a,b, $\phi \approx 200°$) was notably different for the two configurations. The initial amplitude of the fan upstream pulsations was slightly greater for the counter-rotating configuration due the increase in blade incidence angle (Fig. 11) produced by the counter-swirl towards the tip of the fan blade. On the other hand, for the co-rotating configuration the amplitude of the fan perturbations increased towards mid-span of the blade (Fig. 10a,b, $\phi \approx 200°$) due to the opposite blade incidence angle distribution compared to the counter-rotating configuration. Under both conditions, the blade had a notable negative to positive variation in blade incidence angle towards the tip as well as spanwise variation (Fig. 11) that are a possible source of dynamic stall inception (Giuliani and Chen [2016]). The amplitude of the perturbations from the fan decayed further upstream from the AIP (Fig. 10c,d) but the difference in the signature between the two configurations was still notable and it primarily showed a phase shift in the azimuthal direction relative to the AIP. The latter was related to the propagation speed of the upstream finite pressure waves that originate in the fan relative frame of reference.

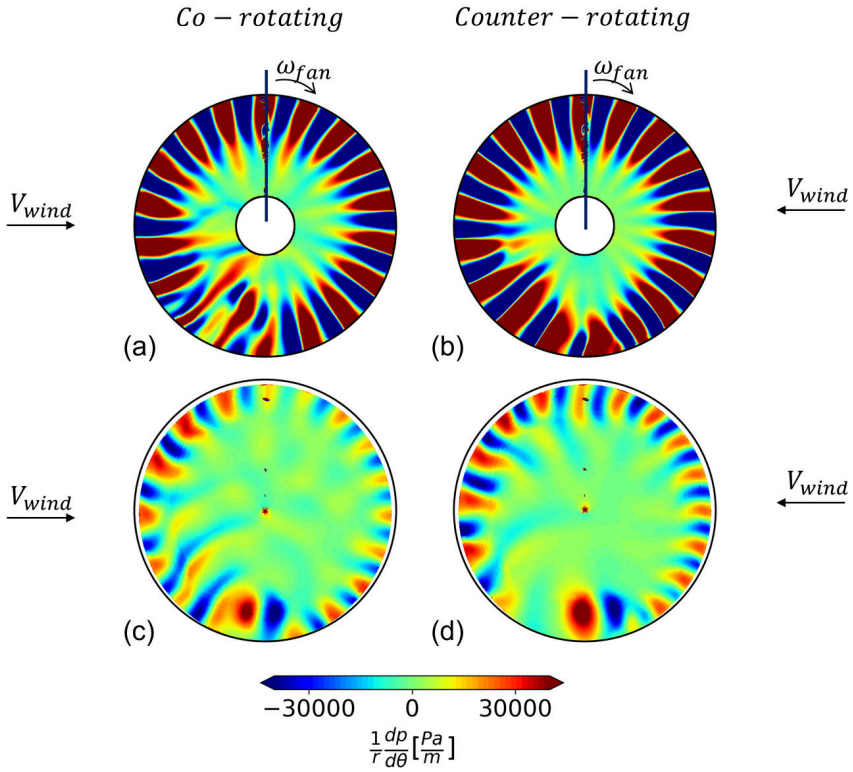

Figure 10: **Effect of crosswind direction on the azimuthal pressure gradient distribution at (a),(b) the AIP and (c),(d) at the intake throat ($\approx 0.4r_{fan}$ upstream of the AIP). Time snapshots for the URANS-TRF model at $V_{wind} = V_{wind,c}$**

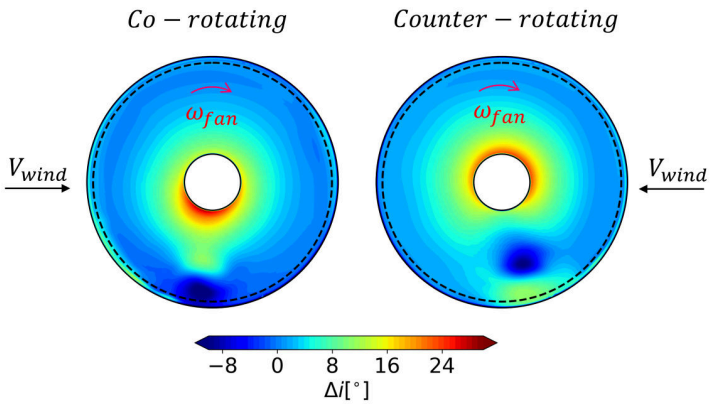

Figure 11: **Effect of crosswind direction on the blade incidence angle distortions at the AIP. Time-average URANS-TRF at $V_{wind} = V_{wind,c}$**

Moreover, the shock signature on the intake lip is on the opposite side for the co-rotating configuration relative to the counter-rotating one (Fig. 12). For the co-rotating configuration, the fan firstly crosses the ground vortex and then the low total pressure region due to the thicker boundary layer which results from the interaction with the shock on the intake lip. The opposite

is true for the counter-rotating configuration. As a results of the different flow topology within the intake and the opposite swirl distortion due to the ground vortex onto the rotor, the decay of the blade-passing pulsations and the modulation of the amplitude of the shock wave on the intake lip was notably different for the two cases. Under the counter-rotating configuration, the shock interacted with the fan upstream pulsations around the topline region ($\phi = 0°$, Fig. 12). On the other hand, for the co-rotating configuration the whole shock front was affected by the azimuthal variation of the static pressure field due to the fan (Fig. 12). For an intake under crosswind with ground interaction the pre-shock Mach number on the intake lip is typically greater around the sideline ($\phi = 90°$) and on the lower intake quadrant ($90° < \phi < 180°$). Thus, for the counter-rotating configuration the interaction between the shock and the upstream fan pulsation was more benign in nature compared to the co-rotating case. Overall, the adverse effect of the unsteady fan-intake interaction on the threshold crosswind speed of the intake was amplified under the co-rotating configuration (Fig. 8).

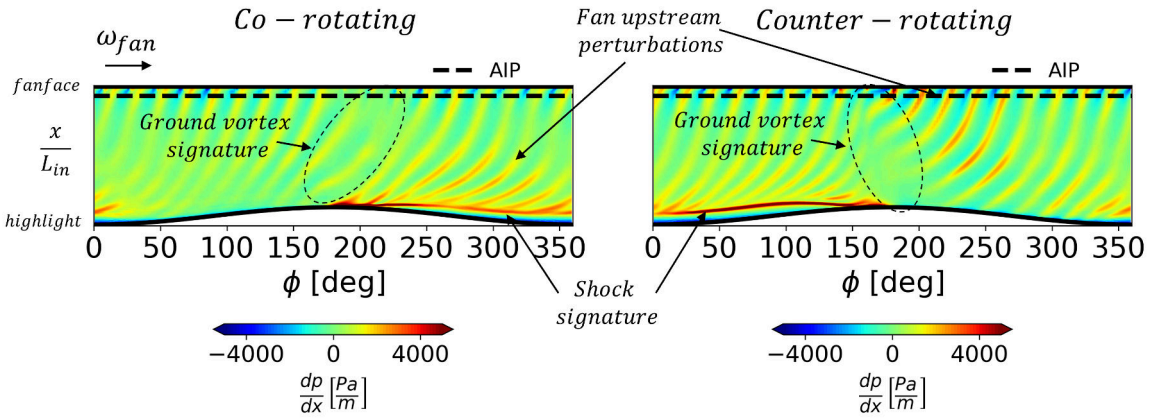

Figure 12: **Effect of crosswind direction on the axial static pressure gradient on the unwrapped intake surface. Time snapshots for the URANS-TRF at $V_{wind} = V_{wind,c}$**

The different upstream propagation of the fan perturbations (Fig. 10) contributed to a notable difference of the spatial distribution of the blade passing frequency signature ($f/f_{bp} \in [0.94, 1.12]$) on the spectrum of the axial static pressure gradient (dp/dx) for both the threshold (Fig. 13) and post- threshold conditions. Compared to the counter-rotating configuration, for the co-rotating one the azimuthal extent and amplitude of the fan upstream pulsations that reached the shock front was notably greater. On the other hand the signature due to the shock unsteadiness (Fig. 13, $f/f_{bp} \in [0.01, 0.19]$) was lower in amplitude for the co-rotating configuration due to the $6kts$ lower crosswind speed which contributed to a lower loading on the intake lip, reduced pre-shock Mach number and reduced ground-vortex circulation. In addition, for the co-rotating case the unsteady signature of the axial static pressure gradient at blade-passing frequency (Fig. 13, $f/f_{bp} \in [0.01, 0.19]$) had an azimuthal wavelength at the shock location that was about twice the blade pitch angle. This confirmed previous findings (Boscagli et al. [2022]) relative to a modulation both in space and time of the intake flow field due the unsteadiness of the fan. Thus, the unsteady coupled interaction between the fan and the intake requires investigations at the early stage of the intake design process. Also, although the effect of vortex-induced distortions on fan performance has been widely discussed in the literature

(Pardo et al. [2014], Page et al. [2018], Awes et al. [2020]), the decay of the amplitude of the upstream pulsation from the fan under co- and counter-rotating vortices is a novel contribution of this research and it will require further investigations to understand how this behaviour is related to the likely change in the radial distribution of the blade loading.

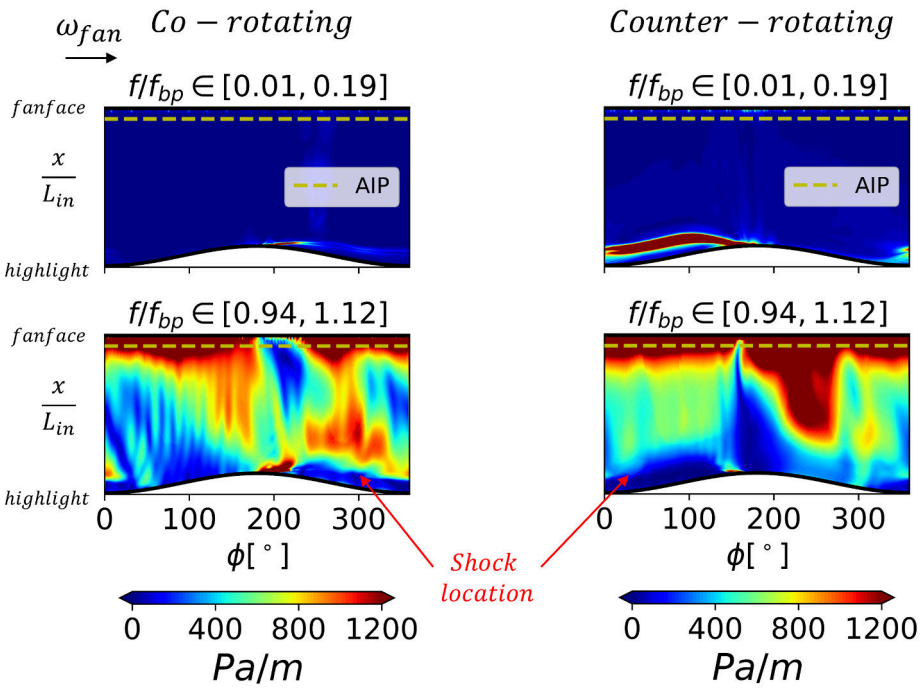

Figure 13: **Effect of crosswind direction on the fluctuations of the axial static pressure gradient on the unwrapped intake surface at blade passing frequency ($f/f_{bp} \in [0.94, 1.12]$). URANS-TRF at $V_{wind} = V_{wind,c}$**

CONCLUSIONS

The impact of fan rotational speed and wind direction on the threshold conditions of a short intake was assessed. Despite the attempt to reduce the amplitude of fan upstream pulsations through a change in fan rotational speed, the intake threshold condition was not affected. The notable increase in fan blade loading due to the distortions generated by the ground vortex dominated the amplitude of the fan upstream pulsations and their adverse effect on the shock on the intake lip. The direction of the wind for a short intake under crosswind conditions is of notable importance as it establishes the direction of rotation of the ground vortex relative to the fan. However, for this case study with an aggressive short intake design and with a prototype low speed fan, the results showed that a vital consideration is the azimuthal phase of the fan perturbations relative to the location of the shock on the intake lip. The interaction between the ground vortex and the fan had the greatest adverse impact on the intake boundary layer for the co-rotating case. Overall, the adverse effect of fan unsteadiness and the unsteady interaction between the fan, ground vortex and the shock on the intake lip had a dominant role. These considerations and the fact that the reduced order fan model typically overestimates

the efficiency losses through the fan due to the shock in the blade passage indicate that full unsteady fan-intake coupled analyses are needed at an earlier stage of the intake design process. However, it is acknowledged that these studies lack a complete computational model validation with experimental data to corroborate some of the findings, and the effect of a change in the details of intake or fan design was not assessed and therefore their impact is still unknown. Furthermore, the restrictive separation criteria that was used to identify the threshold crosswind speed may be more sensitive to changes in crosswind direction compared to the accepted total pressure distortion parameters used by industry (e.g. DC60 and SAE ARP1420 parameters).

ACKNOWLEDGEMENTS

The doctoral studies of Luca Boscagli were partially funded by Rolls-Royce, plc., and the Engineering and Physical Sciences Research Council (industrial case award 16000032). Robert Christie was partially funded under the Aerospace Technology Institute (ATI)/Innovate UK programme FANFARE.

DATA AVAILABILITY STATEMENT

Due to commercial confidentiality agreements the supporting data are not available.

REFERENCES

A. Awes, A. Brosse, G. Dufour, X. Carbonneau, and B. Godard. Effect of a vortex distortion on the operability of an ultra high bypass ratio fan. *Proceedings of the ASME Turbo Expo*, 2A-2020:1–11, 2020. doi: 10.1115/GT2020-14596.

L. Boscagli, R. Christie, D. MacManus, and T. Piovesan. Aerodynamics of a short intake in crosswind. *Aerospace Science and Technology*, page 107826, 2022.

O. Bron. *Numerical and experimental study of the shock-boundary layer interaction in transonic unsteady flow.* Phd thesis, KTH Royal Institute of Technology, 2002.

T. Cao, P. Hield, and P. G. Tucker. Hierarchical immersed boundary method with smeared geometry. In *Journal of Propulsion and Power*, volume 33, pages 1151–1163. American Institute of Aeronautics and Astronautics Inc., 2017a. doi: 10.2514/1.B36190.

T. Cao, N. R. Vadlamani, P. G. Tucker, A. R. Smith, M. Slaby, and C. Sheaf. Fan-Intake interaction under high incidence. *Journal of Engineering for Gas Turbines and Power*, 139 (4):1–10, 2017b. ISSN 15288919. doi: 10.1115/1.4034701.

M. Carnevale, F. Wang, and L. Di Mare. Low Frequency Distortion in Civil Aero-engine Intake. *Journal of Engineering for Gas Turbines and Power*, 139(4), 2017. ISSN 15288919. doi: 10.1115/1.4034600.

J. Cui, R. Watson, Y. Ma, and P. Tucker. Low order modeling for fan and outlet guide vanes in aero-engines. *Journal of Turbomachinery*, 141(3):1–9, 2019. ISSN 15288900. doi: 10.1115/1.4042202.

J. E. Giuliani and J. P. Chen. Fan response to boundary-layer ingesting inlet distortions. *AIAA Journal*, 54(10):3232–3243, 2016. ISSN 00011452. doi: 10.2514/1.J054762. URL `https://doi.org/10.2514/1.J054762`.

C. A. Hall and T. P. Hynes. Measurements of intake separation hysteresis in a model fan and nacelle rig. *Journal of Propulsion and Power*, 22(4):872–879, 2006.

B. Hodder. An investigation of possible causes for the reduction of fan noise in flight. *3rd Aeroacoustics Conference*, page 585, 1976.

L. Lapworth. Hydra-CFD: a framework for collaborative CFD development. In *International conference on scientific and engineering computation (IC-SEC)*, volume 30, 2004.

K-B. Lee, M. Wilson, and M. Vahdati. Effects of Inlet Disturbances on Fan Stability. *Journal of Engineering for Gas Turbines and Power*, 141(5), may 2019. ISSN 0742-4795. doi: 10.1115/1.4042204.

Y. Ma, N. R. Vadlamani, J. Cui, and P. Tucker. Comparative studies of RANS versus large eddy simulation for fan-intake interaction. *Journal of Fluids Engineering, Transactions of the ASME*, 141(3):1–13, 2019. ISSN 1528901X. doi: 10.1115/1.4041393.

M. Migliorini, P. K. Zachos, and D. G. MacManus. Novel Method for Evaluating Intake Unsteady Flow Distortion. *Journal of Propulsion and Power*, pages 1–13, 2021. doi: 10.2514/1.b38127.

P. Moinier. *Algorithm developments for an unstructured viscous flow solver*. Phd thesis, Oxford University, 1999.

J. P. Murphy and D. G. MacManus. Ground vortex aerodynamics under crosswind conditions. *Experiments in Fluids*, 50(1):109–124, 2011. ISSN 07234864. doi: 10.1007/s00348-010-0902-4.

J. H. Page, P. Hield, and P. G. Tucker. Effect of inlet distortion features on transonic fan rotor stall. *Journal of Turbomachinery*, 140(7):1–11, 2018. ISSN 15288900. doi: 10.1115/1.4040030.

A. C. Pardo, A. Mehdi, V. Pachidis, and D. G. MacManus. Numerical study of the effect of multiple tightly-wound vortices on a transonic fan stage performance. In *Turbo Expo: Power for Land, Sea, and Air*, volume 45578, page V01AT01A033. American Society of Mechanical Engineers, 2014.

C. Reid. The response of axial flow compressors to intake flow distortion. *Proceedings of the ASME Turbo Expo*, 1A, 1969. doi: 10.1115/69-GT-29.

P. R. Spalart and S. R. Allmaras. One-equation turbulence model for aerodynamic flows. *Recherche aerospatiale*, (1):5–21, 1994. ISSN 00341223. doi: 10.2514/6.1992-439.

L. G. Trapp and R. Da Motta Girardi. Crosswind effects on engine inlets: The inlet vortex. *Journal of Aircraft*, 47(2):577–590, 2010. ISSN 15333868. doi: 10.2514/1.45743.

N. R. Vadlamani, T. Cao, R. Watson, and P. G. Tucker. Toward future installations: Mutual interactions of short intakes with modern high bypass fans. *Journal of Turbomachinery*, 141 (8):1–11, 2019. ISSN 15288900. doi: 10.1115/1.4044080.

B. G. Van Der Wall and H. Richard. Analysis methodology for 3C PIV data. *31st European Rotorcraft Forum*, 2005, 2005.

S. Zantopp, D. MacManus, and J. Murphy. Computational and experimental study of intake ground vortices. *Aeronautical Journal*, 114(1162):769–784, 2010. ISSN 00019240. doi: 10.1017/S0001924000004255.

Fan-intake aerodynamic interactions under crosswind conditions

Boscagli, Luca

2023-04-28

Boscagli L, MacManus DG, Christie R. (2023) Fan-intake aerodynamic interactions under crosswind conditions. In: 15th European Conference on Turbomachinery Fluid dynamics & Thermodynamics, 24-28 April 2023, Budapest, Hungary

https://doi.org/10.29008/ETC2023-303